CHAPTER 4

FABRICATION OF A FIBER SCANNER PROBE FOR SPECTROSCOPY

Highlights of the Chapter

- *Video-rate fiber scanner probe is fabricated for spectroscopy.*
- *Use of 3D printed parts in place of custom ceramic one reduced cost and retained the quality factor of scanner.*
- *Stability study and initial imaging of florescence beads reveals the high probability of scanner suitability in clinical setup for point of care instruments.*

Abstract:

Resonant fiber laser scanners enable an elegant means to perform laser scanning microendoscopy in a compact probe device. These are on the order of a few millimeters in diameter, which is ideal for insertion into the working channel of a standard clinical endoscope. However, a significant source of complexity is to micromachine the traditionally used ceramic piece to mount the fiber optic within the piezoelectric tube, and to achieve video rate at the fundamental resonance frequency is not possible without the severe restriction of the field-of-view of the scanner. Here, we introduce methods to simplify the fabrication of fiber scanners using 3D printed parts and achieve video-rate imaging while maintaining the field-of-view of the scanner utilizing the higher-order harmonic oscillation beyond the conventional use of the fundamental frequency. We present the design, the simulation, the stability achieved, and the empirical

performance of the low-cost, high-speed double-clad fiber resonant scanner. The approaches described here result in stable scan patterns (<6 μm shift in 84 hours) at frame rates up to 20 fps.

4.1. Introduction

Imaging of internal organs plays an important role in prognosis and diagnosis of different physiological and pathological conditions. In-vivo imaging along with several benefits, comes with inherent challenges like inaccessibility of inside parts of living organisms. This requires development of such a technique to image in-vivo to understand the functioning of the organisms. Internal organ imaging can be categorized broadly in two groups: (a) Structure-based imaging (b) Surface based imaging. Surface based imaging provides high resolution visualization of internal organs. Multiphoton microendoscopy (MPM) is one such tool which is a fluorescence imaging technique that allows the non-invasive and in-vivo study of intact live tissue in three dimensions to sub-micrometer level below the surface [1-5] where near-infrared femtosecond lasers are used to excite fluorophores. Two-photon excitation fluorescence (TPEF) is an example of such a process in which a fluorophore is excited by simultaneous absorption of two near-infrared photons [6]. TPEF is a primary signal generated in a multiphoton microendoscopy.

Conventional endoscope diameter is approximately equal to thickness of human finger and used for in vivo color imaging of internal organs. The disadvantage of this technique is size and poor image quality. To overcome this, a scanning fiber endoscope (SFE) is used where the fiber cantilever is actuated to move in a spiral pattern to acquire images. Proximal and distal scanning systems are generally used for scanning SFE depending upon the relative position of the excitation source from the scanner [7]. Proximal scanners use coherent fiber bundles while distal scanning systems use single optical fiber for light delivery and collection [8]. Distal scanners may adopt an electromechanical system (MEMS) of mirror scanners or a resonant fiber optic piezoelectric

scanner [9][10]. Electromechanical scanners, being expensive and delicate to fabricate, have large-size MEMS mirrors and control circuits which limits the miniaturization of the probe. An alternative option is to use resonant fiber optic scanners which can be miniaturized in the range of 1.5 – 2 mm or even less [11] [12].

In the year 2000, the concept of delivering excitation light using single fiber in vibratory resonance and detecting back the resultant light was proposed which over the time improved. Compared to a coherent fiber bundle where light is acquired in parallel, SFE acquires light in one pixel at a time or time series pattern. A custom SFE in general consists of a piezo tube and an optical fiber. The optical fiber is fixed at the distal end of the piezo tube to obtain a fiber cantilever. The piezo is driven at a resonant frequency of the fiber cantilever. Mechanical resonance gain allows the small vibration of a piezo tube to vibrate the tip of the fiber cantilever with amplification of a hundred times. The piezo tube is divided in four quadrants and a pair of opposite quadrants is supplied with amplified sine wave actuation while another pair of quadrants is supplied with cosine wave to obtain circular pattern. Scanning pattern is obtained by regulating the amplitude of actuation voltage.

In the last two decades, a huge number of fiber optic scanning micro endoscopes have been prototyped. Major developments were achieved by different groups working in the field which can be broadly divided into three categories: 1) Fiber cantilever for delivery of pulse laser and receiving excitation signals 2) High NA micro-objective lens system for efficient collection of image signals and tight focusing of the laser on sample, and 3) Compact beam scanning mechanism for image formation. Myaing et. al. (2005) developed a miniature endoscope using piezoelectric tube and double-clad fiber. Real-time imaging of fluorescent beads and cancer cells have been successfully performed. Harzic et. al. (2008) used hollow core photonic crystal for illumination.

Developed probe had a field-of-view of 420 um x 420 um and demonstrated the ability of the system to image cellular details. Tang et. al (2009) illustrated the use of two-axis MEMS mirror and double-clad photonic crystal fiber for microendoscope fabrication. A two-lens system including a collimation lens and a focusing lens was used and applied to image fluorescent microspheres and bovine knee joint cartilage. Another group (Rivera 2011) developed a 3 mm outer diameter flexible endoscope for TPEF using resonant/non-resonant fiber raster scanner and GRIN lens assembly and image obtained for unstained tissues. Zhang et. al. (2012) developed an all-fiber optic scanner which was capable of high-resolution second harmonic generation imaging and had an outer diameter of 2 mm. The developed probe is used to assess abnormal cervical remodeling associated with preterm birth. Guillaume et. al. (2015) developed a miniaturized fiber scanner with custom-made double-clad polarization maintaining photonic crystal fiber of outer diameter 2.2 mm. The probe allows simultaneous imaging of second harmonic generation and two photon excited fluorescence with a frame rate of 8 fps and with field of view of 450 um. Zong et. al. (2017) designed a fast high resolution two photon microscope where hollow-core photonic crystal fiber delivers a 920 nm femtosecond laser in raster scanning. Ang Li et. al. (2019) developed a biopsy needle compatible rigid probe with outer diameter of 1.75 mm and field of view of 120 um. Several other scanners were developed which outperformed its precursor versions.

TPEF has a number of advantages such as intrinsic optical sectioning, reduced photobleaching and phototoxicity, lesser background signal, and enhanced depth of penetration making it a suitable tool for in-vivo biomedical imaging applications [13] [14]. Additionally, the wavelength of the excitation laser source is usually in the infrared region, far away from visible TPEF signal, thus, it can be suppressed easily by a filter, giving less background noise for the

detectors. However, the translation of TPEF to a clinical setup has many challenges. The cost and lead time required to obtain and micromachine the conventional ceramic piece used to mount the optical fiber makes the fabrication process of the probe complex. Achieving video-rate imaging is another issue in TPEF based microendoscope systems because of difficulty in gathering images at a high frame rate owing to lack of data acquisition speed in the point-by-point-based image collection.

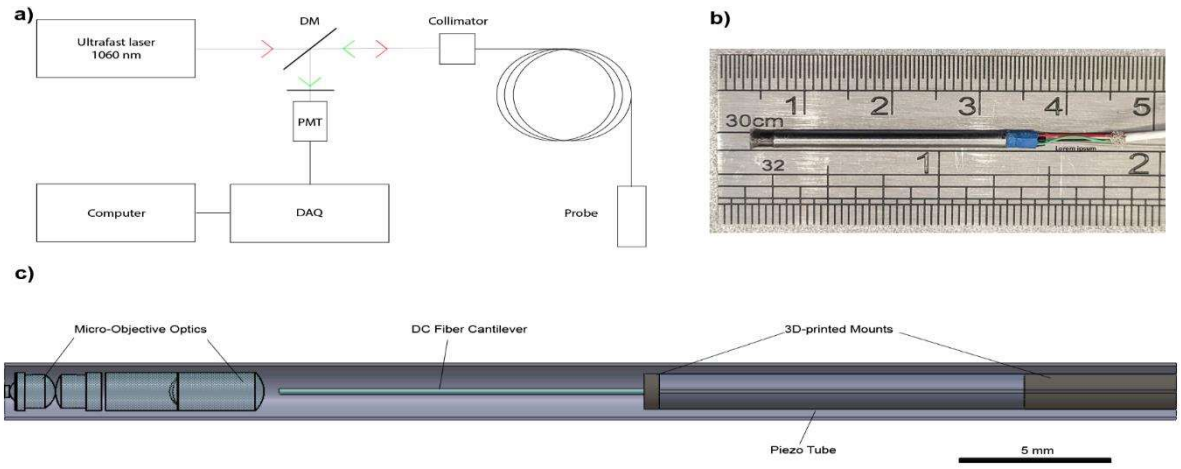

Figure 4.1: General overview of endoscope (a) Schematic of complete system (b) Fabricated microendoscope (c) Solid works cross view of microendoscope showing internal structures

We present the use of a 3-D printed mount to couple the fiber cantilever to the PZT. Previously, a ceramic part was used for coupling. Its high cost of manufacturing (around $500) and the fact that it has to be custom made cause the lead time to obtain it to increase up to several weeks in comparison to cheaper (under $5) 3-D printed mounts with negligible lead time. Also, a Fiber cantilever is required to oscillate at resonance frequency so that maximum deflection is obtained for a larger field of view. If natural frequencies of oscillation are known, we can actuate the fiber cantilever near to these frequencies so that resonance occurs [19]. ANSYS is used here to study the natural frequency and harmonic response of the fiber cantilever. To increase the frame rate of the microendoscope to 20 fps, a relatively large vibration frequency is required to scan

evenly over the field of view. Therefore, the first harmonic resonance frequency of the cantilever is used instead of the fundamental frequency. We also tested the stability of the fiber scanner by collecting 84 hours of continuous data, and proved that the fiber scanner is stable for both short term (frame-to-frame) and long term (during the operation period).

4.2. Material and Methods

4.2.1 Piezoelectric Tube

A PZT (Physik Instrumente GmbH & Co., Germany) can produce a small positional change in the nanometer range for a slight change in operating voltage. PZTs are used in scanning fiber microendoscope probes to provide dynamic scanning actuation to the fiber cantilever. PZT actuator is made of a monolithic PZT with the inner surface as common ground and the outer surface divided equally into four conductive quadrants. Each pair of opposite quadrants are connected to a differential voltage signal generated from a custom LabVIEW program via National Instrument Data Acquisition (DAQ) device and amplified by the PZT drivers provided by Physik Instrumente. This makes one side of the PZT shrink and the other side expands causing the PZT to bend. The capacitive impedance of PZT electrodes is very high due to which signal current stays in the range of milliamperes (average up to 40 mA) making it safe for endoscopic application [16]. A double-clad fiber (P-6/125DC, Thorlabs) goes along the axis of the PZT and is coupled with the ends of PZT by 3D printed mounts. When a periodic voltage signal is applied, the PZT vibrates in the corresponding direction. The force due to the mechanical position change of the PZT is transferred to the fiber cantilever causing it to vibrate with a similar pattern. Hence, driven by the custom modulated signal, the fiber can vibrate in the desired pattern.

The schematic diagram of a video-rate low-cost microendoscope is illustrated in fig 1(a). It consists of a double-clad fiber-optic cantilever coupled to a piezoelectric tube (PZT) actuator by

3D printed parts. The outer surface of the PZT actuator is divided into four quadrants to form two pairs of actuation electrodes [15-16]. Ideally, sinusoidal actuation voltage is applied to the two pairs of electrodes with one pair of voltage shifted in phase by 90 degrees [17]. This causes the PZT to bend with respect to quadrants causing the fiber cantilever to move. Although the PZT has inherently small displacement (few micrometers max.), a large scan amplitude can be obtained if the fiber oscillates at its resonance frequency. The PZT actuator has a cylindrical geometry and can be fabricated into small dimensions (outer diameter up to 1mm) which is perfect for miniaturized scanners.

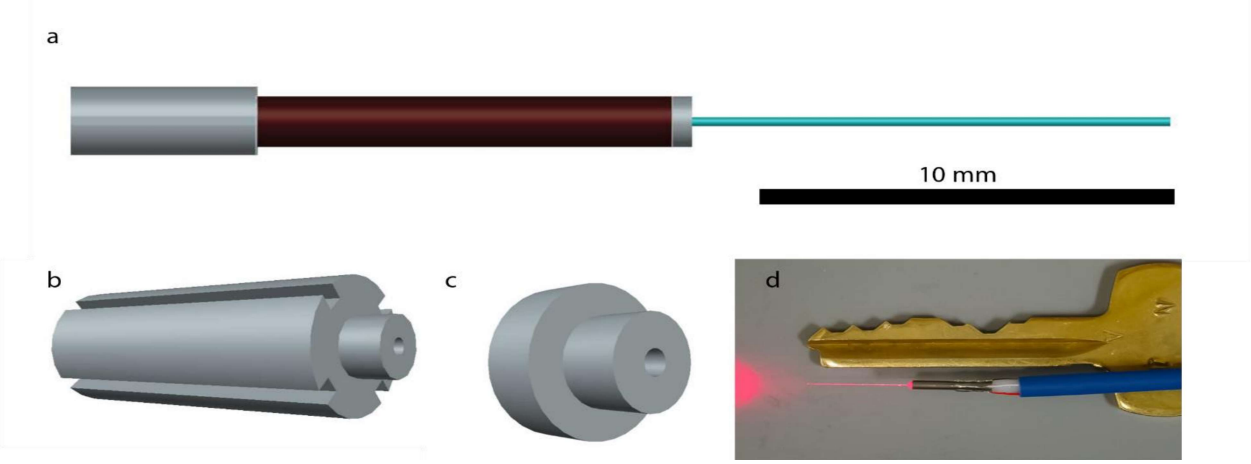

Figure 4.2. AutoCAD model (a) Complete probe (b) lower mount having a groove for PZT wire take out (c) front mount used for coupling PZT with fiber cantilever (d) Actual fiber probe.

4.2.2 3-D Printed Mount

For our probe, 3-D printed mounts are fabricated using Stratasys Eden 260v with PMMA material. Two different parts are fabricated for opposite ends of the PZT. Figure 4.2(b) shows the mount which is used for fixing PZT-fiber assembly to a metal tube on which grooves are made to accommodate PZT driving signal wires. The 3-D printed mount in figure 4.2(c) is used to couple the mechanical vibration actuated in PZT to the fiber cantilever. The outer diameter of this part is

equal to the outer diameter of PZT (1.5 mm). The center of the mount is drilled to fit the double-clad fiber of which coating is removed. To drill a hole for the fiber accommodation, a 250 μm drill is used which works best for the fiber used in the probe and then the fiber is fixed to it with super glue (3M Scotch Weld). The quality and reliability of scanners mainly depend on two mechanical components - the mount which sets the position of the scanner within the tube and the mount which couples the PZT movement to the fiber [18]. To retain the repeatability in the fabrication of the 3-D printed part, multiple mounts are fabricated in a single model. The mount that holds the base of the fiber cantilever has a direct influence on the resonant frequency of the system. Mounts should be designed in such a way that it is able to securely hold the position while allowing the PZT to vibrate. The mounts are glued and thus the position of the fiber cantilever cannot be adjusted thereby fixing the resonant frequency of the system.

4.2.3 Fiber Cantilever

Mechanical vibration in the PZT is transferred to the fiber cantilever which acts as an excitation light delivery medium. Field of view (FOV) for the probe depends on the maximum deflection of the fiber tip upon driving at the resonance frequency. Also, the speed of image acquisition depends on the time duration required by the fiber cantilever to complete one scan. In order to improve radial resolution and avoid excessive stress on the fiber cantilever caused during vibration, higher-order harmonic resonance frequency is used instead of the fundamental resonance frequency.

The resonance frequency of a cylindrical structure is given by

$$Fr= 2\pi L2EI\rho A$$

where L is the length of the fiber cantilever, E and ρ are Young's modulus and mass density respectively; β is a constant determined by vibration mode number [20]. For the probe we

fabricated, β for the fundamental resonance frequency and the first harmonic is 3.52 and 22.4 respectively [21]. Two models of fiber cantilever were modeled in AutoCAD of length 4.5 mm and 11.3 mm. These lengths were selected as the fundamental resonance frequency for 4.5 mm fiber and 1st harmonic resonance frequency for 11.3 mm fiber was approximately the same (around 4.8 kHz). Models were imported in Ansys on which and modal and harmonic response analyses were done to see the stress and tip displacement relation. The fiber was modeled as a 125 μm cylinder. One end of the fiber cantilever is fixed in the study. The model is meshed using the program control and a total of 495 elements and 2594 nodes were obtained for 4.5 mm fiber and a total of 1221 elements and 6422 nodes were obtained for 11.3 mm fiber which is sufficient to produce a statistically acceptable result. The material used for simulation is pure silica glass with a density of 2700 kg/m3, Young's modulus of 73 GPa, and Poisson's ratio of 0.17. Figure4.2(a) shows the completed probe with wires to deliver the excitation voltage to PZT. Figure 3.2(b) depicts the 3-D printed parts used to couple the fiber cantilever with PZT. The fiber cantilever can be actuated at its fundamental resonance frequency or at the higher-order harmonic frequency to have a maximum deflection of the fiber. Typically, a fiber cantilever of 12 mm length has a fundamental frequency of around 768 Hz and a 1st harmonic frequency of around 4.5 kHz. A faster oscillating fiber cantilever will be able to scan over the field of view at a higher rate thus increasing the frame rate of the system while maintaining the shape of the scanning pattern.

4.2.4 LabVIEW Control Program

To drive the fiber scanner, a pair of the differential voltage signals is generated by DAQ, which is controlled by a custom-made LabVIEW program. The program is capable of generating and mixing modulated sine wave signals in two different channels, which corresponds to the two perpendicular electrode pairs of the PZT. In order to make the tip of the fiber vibrate to get a spiral

pattern, the fiber cantilever is driven by the PZT actuation force along the principal axes to oscillate at 1st harmonic resonance frequency and then a linear brake force is applied to stop the oscillation within the time of one frame.

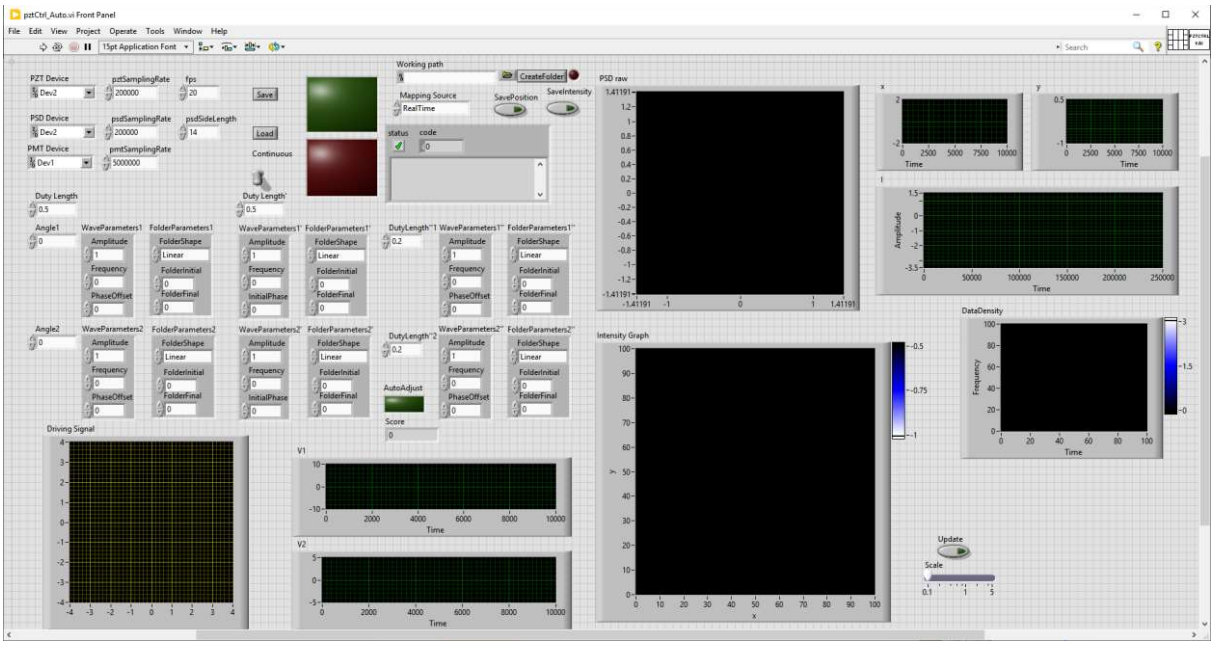

Figure 4.3: GUI for the custom-made signal acquisition and image formation algorithm (LabVIEW)

The GUI of the LabVIEW program. It consists of four regions: the general control (upper left) where the user controls the sampling frequencies and can start/stop the scan, the wave shapes control (middle left) where users define the scanning pattern and create the modulated sine waves, driving signal display (lower left) that plot the electric signal parametrically and as functions of time, and PSD/PMT display (right) where the feedback from the PSD (scan pattern) and the PMT is displayed and plotted in different forms. This screenshot is taken with an ongoing spiral scan.

Due to the imperfection and asymmetry of the fiber cantilever and 3D printed mounts, the resonance frequency differs slightly in two directions. Therefore, simply sending modulated sine waves with 90° phase shift in two perpendicular directions yields an uncontrollable scanning pattern. To control the pattern and apply an effective brake signal, the driving signal must be

applied on the principal axes - the direction where the displacement of the fiber tip is parallel to the driving force. Therefore, if a sine wave signal is applied along with one of the principal axes, the fiber will oscillate in the same direction, otherwise, an oscillation in a 2D elliptical pattern will occur. To achieve driving in any selected direction, the program calculates the components of the driving signal in x and y directions according to user-defined angles and simple trigonometry.

The PZT driving signal consists of two steps: the driving part and the braking part. The driving signal is a linear increasing sinusoidal wave following the equation: $V_i = A_i(t)\sin(\omega_i(t) + \varphi_i)$ where the subscript i stands for the directions of the two principal axes, ω is the natural resonance angular frequency, and φ is the phase shift experimentally determined that creates a circular pattern. The braking signal is a linear decreasing sinusoidal wave that applies 180 degrees out of phase with the velocity of the fiber. Therefore, the PZT equivalently provides a damping force that reduces the oscillation faster than the natural relaxation of the oscillator.

Two steps are required to collect the images: 1) the scanning pattern calibration, and 2) the fluorescence intensity collection. During the scanning pattern calibration, the lens-PSD combination setup is used to measure the motion of the fiber scanner. The XY-displacement of the fiber scanner tip during one scanning frame is measured. This creates an array of position data as the function of time. Then, with the fiber scanner kept running, the endoscope can be applied to bio samples to collect the TPE signal. The signal is collected by the PMT, resulting in an array of fluorescent intensity data as the function of time. The LabVIEW program interpolates the both arrays and yields the intensity as a function of position to generate the endoscopic image.

4.3 Result and Discussion

For the purpose of characterizing the scanner, double-clad fiber with 6.0±0.5 μm mode field diameter, 125±2 μm inner cladding diameter, 245±15 μm outer cladding diameter with core

numerical aperture (NA) of 0.15 is used. A four-channel amplifier is used to drive the PZT configured to give a gain of 25. The operational amplifier is controlled through logical control from USB 6363 (National Instruments, Austin, Texas) analog/digital input-output(I/O) card. The driving system provides actuation voltage in the range of ±100 V in response to the logical signal of ±4 V. To optimize the deflection of the PZT, the opposite pair of quadrants are driven by differential voltage.

Stress and tip displacement is first studied using Ansys. The two modeled fiber cantilever is imported and modal and harmonic analysis is done. Figure 4.3(a) and 4.3(b) Figure number shows stress distribution on fiber structure when the actuation force is kept constant. It can be noted that the maximum stress generated on the fiber is always near the fixed point of the cantilever. Also, the maximum stress generated for 11.3 mm fiber is lower Fig. 4.3(b) than the maximum stress generated for 4.5 mm fiber Fig. 4.3(a). It can be observed from figure 4.3(c), that the maximum tip displacement is much higher for 11.3 mm first harmonic frequency as compared with 4.3 mm fundamental frequency when the maximum stress for both the fibers is kept constant. The fiber cantilever can be made to resonate either at fundamental frequency or at any one of its harmonic resonance frequencies. Figure 4.3(d) shows the variation of fundamental and 1st harmonic resonance frequency as the length of fiber cantilever is varied. For our probe, the length of the free moving fiber cantilever is 12 mm (approx.) for which fundamental frequency is calculated to be nearly 768 Hz whereas 1st harmonic resonance frequency is 4840 Hz approximately.

The characteristics of the scanner at resonance are evaluated by measuring the amplitude of oscillation for the two scan axes as a function of the resonance frequency. Figure 4.3d above shows the measured resonance characteristic of the cantilever for the two driving axes near the 1st

harmonic frequency. In the figure, it can be seen that both axes exhibit sharp resonance around 4880 Hz with distinct peaks. The difference in the peak of resonance arises due to the asymmetric alignment of symmetric components owing to the non-ideal nature of the PZT and the fiber cantilever. It is also observed that the frequency difference is only 0.41% (20 Hz/4860 Hz). Meanwhile, a high Q-factor of the fiber cantilever is desired as it takes less driving force to reach the required amplitude by using resonance. The Q-factor can be measured as the ratio of resonance frequency to its peak width. For the fabricated scanner, Q-factor is determined to be 244 and 286 in the two principal axis directions which are high enough to deduce that the scanner is having good quality and low damping. In comparison, the quality factor of a fiber scanner with a similar structure but using a ceramic mount is typically 240.

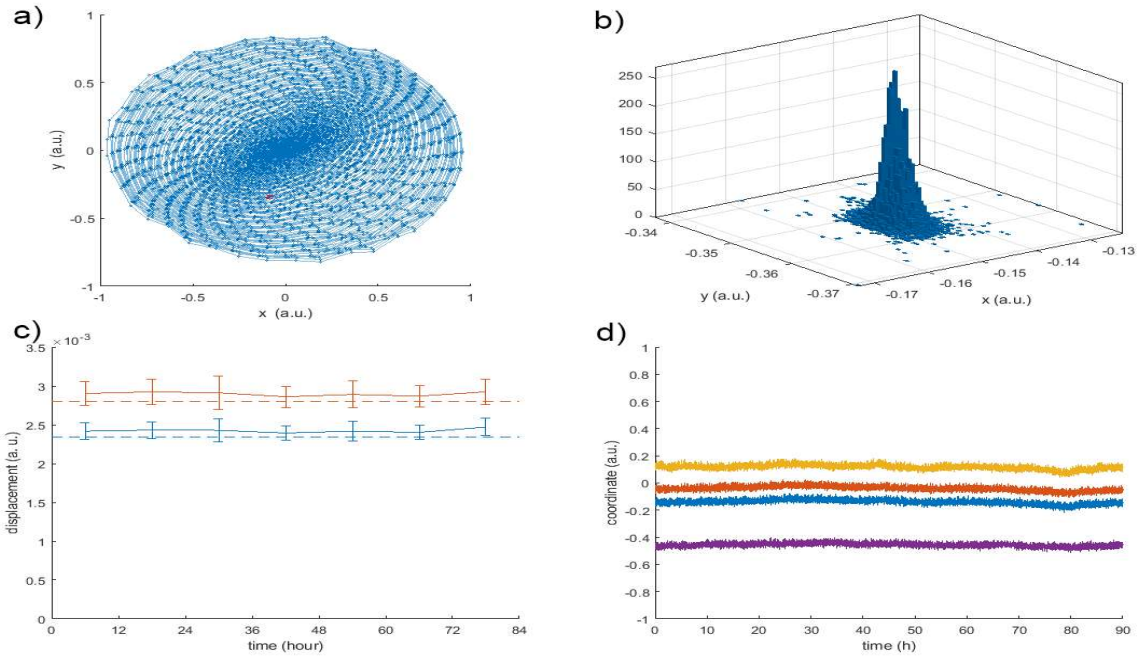

Figure 4.4: Stability study of fabricated endoscope (a) Scanning pattern (b) Short term distribution of single acquisition point in XY plane (c) long term stability of fiber tip (d) Long term stability of four randomly selected points

To test the short-term stability of the fiber scanner, the continuous position data is recorded by the PSD while the fiber scanner oscillates in the spiral scanning pattern during multiple 12-hour runs. On each run, the same scanning pattern is selected and the position data generated from the PSD is recorded. The result is shown in Fig. 4.4 above. To prove the short-term stability, a 2-D histogram of the position of a randomly selected point over a 1-minute scan period is shown. The distribution of the frame-to-frame displacements of a point over time is analyzed. Considering the electrical noise of the PSD, the distribution data is compared with the same data collected when the PZT driving signal is turned off and the fiber scanner stays still.

The following could be understood by seeing the graph Fig 4(c) where the standard deviation of the position of 50 different randomly selected data points in a given frame is plotted for multiple 12 hours runs across a 1-week period. The minimal difference in the standard deviation between the plots when there is no scanning compared to a scan done shows that any cause of disturbance in the stability of the probe is owing to the electrical noise in the position detection by the PSD instead of the instability of the fiber cantilever. One more important point to notice is how the standard deviation in the Y-axis is always higher compared to the standard deviation in the X-axis. This is because of the alignment of the experimental setup particularly to get past the reflections in the light path because of the PSD.

4.4. Conclusion

Here, we presented the use of 3-D printed parts and 1st harmonic resonance frequency for a low-cost and fast fiber scanning probe for TPM. The lead time to obtain the 3-D printed mount is much less as compared to the prior used ceramic part which is custom made and requires weeks of time to procure. Also, the ceramic part is expensive (around 400 $) whereas the 3-D printed part is much more economical (4-5 cents). Also, variation in the scanning pattern can be observed with

varying PZT driving signal parameters which gives an idea of efficient coupling of the PZT and fiber cantilever using a 3-D printed mount. Change in frequency around 1st harmonic resonance frequency was reflected in the scanning patterns as the amplitude of the linear patterns decreased. 3-D printed mounts, as shown in fig. 2(b) & fig.2(c), worked well allowing the vibration of the actuator and transferring the change in the actuation parameters to the scanning pattern. ANSYS simulation is done to obtain an approximate range of frequency where the fiber cantilever shows resonance. The PZT actuation signal is then modulated and adjusted near to these frequencies so that the fiber cantilever oscillates in resonance giving maximum deflection of the tip. Either fundamental resonance frequency or first harmonic resonance frequency can use for oscillation of the fiber. The fundamental resonance frequency is obtained near to 607 Hz whereas the first harmonic resonance frequency comes around 3840 Hz. The first harmonic frequency decreases the scan duration per frame allowing image acquisition at video rate around 20 frames per second retaining stable scanning patterns as shown in Fig. 4. From the above discussion, one can conclude that the 3-D printed mount in conjunction with the use of first harmonic frequency can be used to have a stable low-cost fiber probe with video-rate image acquisition.

References

[1] Zhang, W., Noble, J. A., & Brady, J. M. (2006, April). Real time 3-D ultrasound to MR cardiovascular image registration using a phase-based approach. In Biomedical Imaging: Nano to Macro, 2006. 3rd IEEE International Symposium on (pp. 666-669). IEEE.

[2] Penney, G. P., Blackall, J. M., Hayashi, D., Sabharwal, T., Adam, A., & Hawkes, D. J. (2001, July). Overview of an ultrasound to CT or MR registration system for use in thermal ablation of liver metastases. Med Image Understanding and Anal (Vol.1,p. 6568).

[3] Lange, T., Eulenstein, S., Hünerbein, M., Lamecker, H., & Schlag, P. M. (2004, September). Augmenting intraoperative 3D ultrasound with preoperative models for navigation in liver surgery. In International Conference on Medical Image Computing and Computer-Assisted Intervention (pp. 534-541). Springer Berlin Heidelberg.

[4] Lange, T., Papenberg, N., Heldmann, S., Modersitzki, J., Fischer, B., Lamecker, H., & Schlag, P. M. (2009). 3D ultrasound-CT registration of the liver using combined landmark-intensity information. International journal of computer assisted radiology and surgery, 4(1), 79-88.

[5] Xie, Z., & Farin, G. (2001). Deformation with hierarchical b-splines. Mathematical Methods for Curves and Surfaces: Oslo 2000, 545-554.

[6] Lee, D., Nam, W. H., Lee, J. Y., & Ra, J. B. (2010). Non-rigid registration between 3D ultrasound and CT images of the liver based on intensity and gradient information. Physics in medicine and biology, 56(1), 117.

[7] Ra, J. B., Lee, D., Kim, Y. S., & Lee, J. H. (2008). Non-rigid registration of 3D ultrasound and CT images in the liver using intensity and gradient information. In Proc. Computer Assisted Radiology and Surgery.

[8] Castro-Pareja, C. R., Zagrodsky, V., Bouchet, L., & Shekhar, R. (2005, May). Automated prostate localization in external-beam radiotherapy using mutual information-based registration of treatment planning CT and daily 3D ultrasound images. In International Congress Series (Vol. 1281, pp. 435-440). Elsevier.

[9] Pluim, J. P., Maintz, J. A., & Viergever, M. A. (2003). Mutual-information-based registration of medical images: a survey. IEEE transactions on medical imaging, 22(8), 986-1004.

[10] Mellor, M., & Brady, M. (2005). Phase mutual information as a similarity measure for registration. Medical image analysis, 9(4), 330-343.

[11] Pluim, J. P., Maintz, J. A., & Viergever, M. A. (2000, October). Image registration by maximization of combined mutual information and gradient information. In International Conference on Medical Image Computing and Computer-Assisted Intervention (pp. 452-461). Springer Berlin Heidelberg.

[12] Bhattacharjee, R., & Saini, L. M. (2015, October). Robust technique for the detection of Acute Lymphoblastic Leukemia. In Power, Communication and Information Technology Conference (PCITC), 2015 IEEE (pp. 657-662). IEEE.